DYNAMIC MODEL REFERENCE CONTROL OF A PMAC MOTOR FOR AUTOMOTIVE TRACTION DRIVES.

P Stewart, V Kadirkamanathan, University of Sheffield, UK.

Keywords: Model-Reference, Automotive, Multivariable.

The permanent magnet AC motor drive (PMAC) is a bilinear closely coupled system subject to saturation due to finite dc supply voltage and current limiting for hardware protection. Model reference control can be applied to the PMAC motor, with PI current controllers tracking the model reference current command values. The finite supply voltage constraint results in degradation of system performance when the current regulators saturate. In this paper, a dynamic model reference controller is presented which includes the current and voltage limits and constrains the magnitude of the current vector command signals, operating the system just within the bounds of saturation. This allows the PI controllers to accurately track the command signals and retain control of the current vector. The contoller ensures the maximum possible dynamic performance of the system. The system and controller is presented and experimentally verified, and the PI controller gains are found by Monte Carlo simulation.

1 Introduction

The surface mounted permanent magnet AC motor operates under two distinct regimes, namely constant torque, and constant power. The boundary between these modes (base speed) is defined by operating conditions where the magnitude of the applied voltage equals the magnitude of the back EMF. The motor under consideration is three phase with a "smooth" rotor with surface mounted magnets, and sinusoidal EMF. The constant torque operation of the PMAC is not a novel subject area [1] [2]. Instantaneous torque control is achieved via current vector control in a transformed orthogonal reference frame. For the PMAC surface mount machine, the d-axis current is controlled to zero to ensure maximum torque-per-amp operation. In order to extend the range of the machine beyond base speed, the performance degradation associated with current regulator saturation must be addressed allowing smooth transition into the constant power region. A series of developments based upon the onset of current errors evolved to enable the extended speed region via the injection of negative d-axis current [5]. The algorithms are extensions of basic feedforward control techniques [3] [4]. Current regulator saturation is detected by increasing errors in the d-axis current, which is very small in the constant power region due to high current regulator gains. The error detection serves to suppress the q-axis current command thus regaining control of the current vector. Steady-state experimental performance confirms the flux-weakening capability of this class of controllers. However, since phase-advance is actuated by current controller saturation, insufficient voltage headroom exists to allow the current vector to *dynamically* follow the maximum torque envelope. A more sophisticated approach [6] [7] [8] [9] has been developed which unlike earlier methods does not rely upon current or voltage feedback from the motor to calculate the appropriate level of d and q-axis current for flux weakening, relying instead on known machine parameters to perform the necessary calculations. The d and q-axis current commands are derived either by real-time solution of the steady-state system equations, or by look-up table. These methods are shown to provide good performance in the flux-weakening region, and under steady-state conditions achieve the maximum torque-per-amp profile. Since the dynamic current components are neglected in the calculation of current commands, no voltage headroom is available to optimally advance the current vector under dynamic conditions. The subsequent degradation in current performance is particularly significant under dynamic no-load conditions such as gear-changing. In this paper, a dynamic model reference controller is presented, which reserves an appropriate amount of inverter voltage to allow the maximum possible torque-speed envelope to be followed under dynamic conditions. State de-coupling is acheived by a non-linear feedback element, and losses reduced in the region below maximum torque by minimising the magnitude of the current vector at all times. For automotive drives applications, this results in maximum performance, and the shortest possible gear change

times via an electronically actuated gearbox.

2 Principles of control

The PMAC motor under study has three phase windings which are distributed to give a sinusoidal back EMF with the phase currents having a separation of 120^o electrical. Applying the d-q transformation [10] transforms the three phase currents and voltages into an orthogonal reference frame rotating synchronously with the rotor flux. The system can be described [11] [12] in this reference frame by three equations

$$V_q = ri_q + \omega L i_d + \omega\lambda + L\left(\frac{di_q}{dt}\right) \quad (1)$$

$$V_d = ri_d - \omega L i_q + L\left(\frac{di_d}{dt}\right) \quad (2)$$

$$T_e = k_t i_q \quad (3)$$

where V_d and V_q are the d and q axis voltages, i_d and i_q are the d and q axis currents, r the phase resistance, λ the back emf constant, T_e the instantaneous torque output, L the phase inductance and k_t the torque constant. The motor operates subject to constraints on voltage and current

$$V^2 \geq V_q^2 + V_d^2, I^2 \geq I_q^2 + I_d^2 \quad (4)$$

where V is the available dc voltage magnitude, and I the maximum current limit magnitude. Considering these constraints, maximum torque per amp operation can be achieved by controlling the d axis current to zero. However a boundary exists known as base speed where the rising back emf equals the supply voltage and no further torque production is possible. The speed range of the motor can be considerably extended beyond base speed by introducing negative d axis current and suppressing the q axis current. The

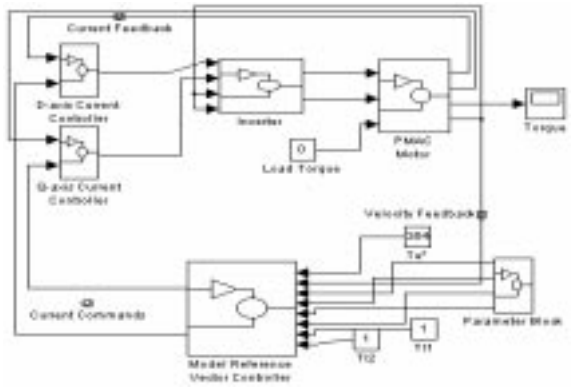

Figure 1: Model reference controller layout.

system layout in figure 1 shows the salient features of the system. It is proposed to utilise a model reference controller outputting d and q axis current commands which are tracked by PI current controllers as part of a feedback linearising controller [13]. The two voltage commands are then converted to three applied phase voltages via the Park transform [11] producing three phase currents in the PMAC. Position and velocity feedback from the motor is obtained from a 12 bit absolute position encoder.

3 Constructing the model reference controller

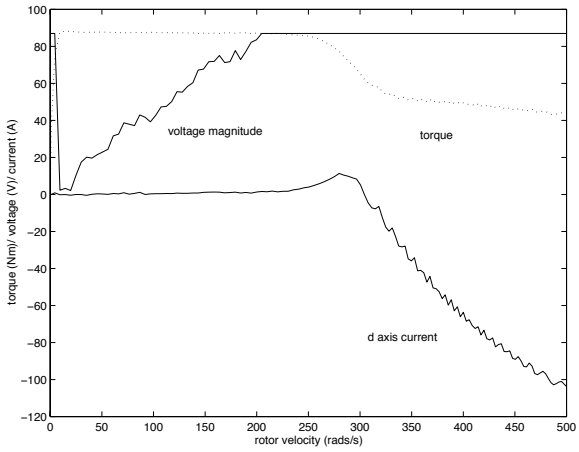

Figure 2: Field weakening controller, dynamic operation, drive motor inertia only. Comparison of d axis current, supply voltage magnitude and produced torque.

The performance shortcomings of existing controller design is demonstrated in figure 2, where the system accelerates under a maximum torque demand and no external load. The controller is a typical field-weakening algorithm relying on current errors to drive the advance of the current vector and is described in [10]. The applied voltage magnitude reaches the DC level of 87 volts, and the current regulators are saturated. Although negative d-axis current is injected, no voltage headroom exists to allow the current vector to follow the optimal field weakening trajectory, and consequently the torque output drops abruptly. The saturation effect is shown in [4], and confirms the simulation results in figure 2. In order to allow the current vector to follow the optimal path and maximise the torque-speed map, a model reference controller is designed to include the current and voltage limitations. Expressions have been derived [13] to describe both the voltage drop due to dynamic effects which is given as

$$V_{drop} = \sqrt{\left(L_s\frac{di_d}{dt}\right)^2 + \left(L_s\frac{di_q}{dt}\right)^2} \quad (5)$$

and also the dynamic base speed associated with this effect which is calculated from

$$0 = -\sqrt{I^2 + \frac{\lambda^2}{L^2}}\omega_b^2 L + V_s\omega_b - \frac{ILk_t\left(L^2I^2 + \lambda^2\right)}{\lambda J} \quad (6)$$

where ω_b is the calculated base speed [13]. In the steady state model reference controller, the current vector I is calculated as extending from $(0,0)$ in the d-q frame to the intersection of the current limit circle and the frequency related voltage limit circle with radius $\frac{V}{\omega L_s}$ and centre $(-\frac{\lambda}{L_s},0)$ as shown in figure 3 The outputs of the model reference are the com-

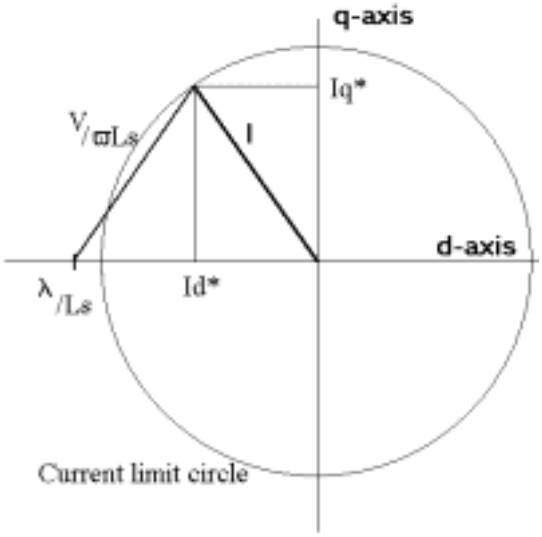

Figure 3: PMAC motor as described by the steady state model reference implementation.

mand quantities i_q^* and i_d^* based on the geometrical representation shown in figure 3. In order to reserve sufficient voltage headroom to allow the current dynamics to act effectively, the length of the voltage limit vector $\frac{V}{\omega L_s}$ must be reduced by an appropriate amount. The voltage reserved for this effect has d and q axis components and can be described as being a vector extending from the voltage limit vector in the model reference as shown in figure 4. The d and q axis current commands are now formulated as the intersection of the dynamic voltage drop (which augments the steady state voltage limit vector) and the current limit circle. For the benefit of reduced computation in the model reference controller, the voltage drop due to the dynamics can be approximated as a worst case. That is the magnitude of the dynamic voltage drop is calculated and subtracted from the magnitude of the voltage limit vector, the new voltage limit vector including the dynamic components being represented as V_{lim}.

$$V_{lim} = \frac{\lambda}{\omega L_s} - V_{drop} \quad (7)$$

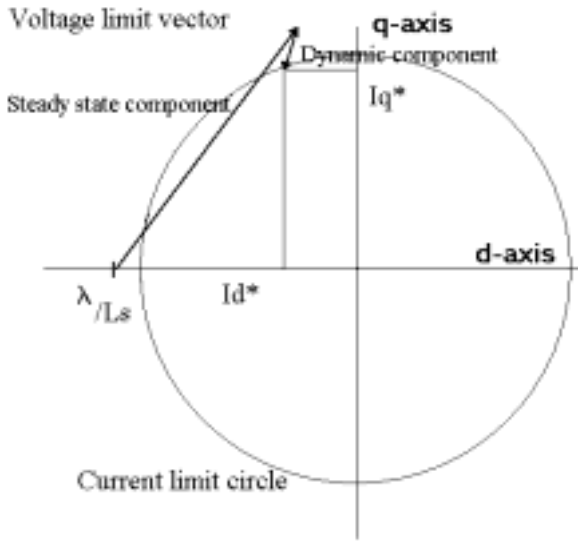

Figure 4: PMAC motor as described by the steady state model reference implementation, augmented by dynamic voltage drop vector.

Similarly, the unmodelled voltage drop due to resistive effects can be included as a worst case effect, and thus the voltage limit vector now contains all the significant system voltage drops, with any minor unmodelled drops being lumped together in the worst case adoption of vector directions. The voltage limit vector now becomes

$$V_{lim} = \frac{\lambda}{\omega L_s} - V_{drop} - r_{drop} \quad (8)$$

where r_{drop} is the unmodelled voltage drop due to resistive effects. If this voltage can be reserved in operation, coupled with a dynamic base speed to enable the reservation process, then the machine should follow the optimal current trajectory with current regulators held just within the bounds of saturation. The geometric implementation in the model reference controller is shown in figure 5. The calculations involved in the implementation of this algorithm are relatively straightforward. In steady state form, the reference model is supplied by a set of memory registers which contain the parameters neccessary to calculate the circle diagram representation with voltage and current limit vectors. The value for dc link supply voltage is measured directly from the dc supply which is either a battery or Ward-Leonard dc generator. Voltage headroom is reserved to include the dynamic and resistive effects by subtraction from the measured DC link voltage, the new value being supplied to the model reference controller. The model reference outputs command values as before and is unaware that voltage has been reserved for dynamic operation. The final part of the implementation is the calculation and use of the revised base speed. An

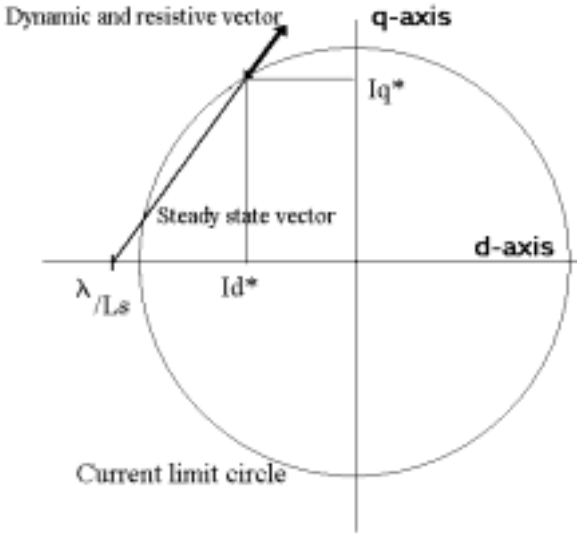

Figure 5: PMAC dynamic model reference control geometric implementation.

expression has been derived to calculate the new dynamic base speed in equation 6. This value is used to switch the voltage reservation algorithm in and out. Below dynamic base speed, the dynamic voltage drop is not subtracted, subtraction only taking place above this new base speed.

4 PI feedback linearising controller

The PMAC motor system equations are cross-coupled an bilinear in its states. Non linear feedback elements must therefore be designed such that accurate tracking of current command signals is achieved. The feedback linearisation schemes described in the literature e.g. [7] are based upon steady state descriptions of the system. In order to decouple and linearise the system for dynamic operation, the existing method has been extended to include the dynamic current errors. The feedback elements are defined as

$$V_d = ri_d - \omega L_s i_q + V_1 L \tag{9}$$

$$V_q = ri_q + \omega(L_s i_d + \lambda) + V_2 L \tag{10}$$

A controller is designed where auxilliary inputs are sybstituted into the non linear feedback elements.

$$V_1 = \frac{di_d^*}{dt} + ki_d^* - ki_d \tag{11}$$

$$V_1 = \frac{di_q^*}{dt} + ki_q^* - ki_q \tag{12}$$

Decoupling of the current loops is achieved, resulting in improved current regulator control, and consequently accurate tracking of the model reference command trajectories. This results in error dynamics of

$$\frac{d\underline{e}}{dt} + k\underline{e} = 0 \tag{13}$$

where

$$\underline{e} = \begin{vmatrix} i_d^* - i_d \\ i_q^* - i_q \end{vmatrix} \tag{14}$$

No rigorous tuning scheme exists to tune the PI gains for the d and q axis current controllers since the system is multivariable and non linear and therefore outside the scope of for example the Ziegler-Nichols tuning method for SISO systems. In practice, the gains are usually tuned on the fly experimentally slowly increasing the proportional gains to achieve good dynamic performance, and then increasing the integral gains to remove any steady state errors that exist. Due to the sharp rise in computational power in even the domestic PC, it has become possible to apply a Monte Carlo analysis of the system to perform a global search to find the optimal gains for dynamic performance. The algorithm must search all combinations of controller gains within bounded values of 0 to 10000 for the proportional gain and 0 to 1000 for the integral gain. A differential term is not included in the controllers due to the presence of current measurement noise and the potential instability which can be introduced. It was initially ascertained through a set of simulations at random gain values that the gain values chosen must be equal in the d and q axis controllers to provide a balanced control action. A simulation was run with the dynamic controller commanding full acceleration for a rotor only inertia from 0 to 400 $rads^{-1}$ for every combination of gains within the search space for a step size of 10. Each simulation produced a waveform of rotor velocity versus torque, and in order to assess performance, each waveform was integrated with respect to velocity to find the PI combination which produces the maximum possible torque speed profile. The wave-

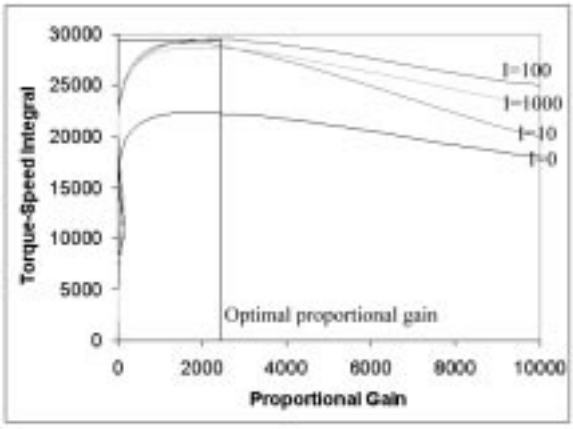

Figure 6: Examples of integral gain performance profiles graphed against proportional gain.

forms shown in figure 6 are a sample of typical output waveforms. The algorithm written in Matlab produces a waveform for each integral gain value versus the entire range of proportional gain values. For each waveform, the maximum value is found, for example in the diagram an optimal proportional gain is found for an integral gain of 100. These results are then correlated to find the optimal PI pair, which was found to be $P = 2000$ and $I = 110$. These are the values which were used for the subsequent experimental verification, and correlated closely with the gain values found experimentally.

5 Experimental verification of the model reference controller

The algorithms proposed were implemented on an experimental test rig with motor parameters: $L_s = 1mH$; $R = 22m\Omega$; $k_e = 0.23V/rad/S$; $t_e = 0.44Nm/A$; $J_{rotor} = 0.017s$; $J_{load} = 0.41s$; $V_s = 87V$; $I_{max} = 200$. In each dynamic simulation and experimental

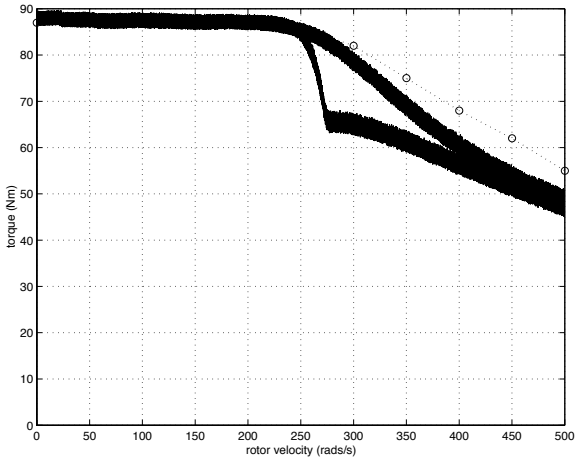

Figure 7: Experimental torque profiles of the steady state and dynamic controllers, compared to the maximum achievable torque profile, connected to external load.

verification, a maximum torque demand causes the rotor to accelerate from rest. the dynamic model reference controller is tested against both rotor inertia alone, and also the rotor connected to an external load motor. The motor torque output is calculated from the measured q-axis current. In figure 7, dynamic and steady-state controllers operating dynamically are compared to the maximum achievable torque-speed profile. The motor is connected to an external load in this case. The profile of the steady-state controller declines rapidly at base speed due to the unmodelled voltage drop and incorrectly calculated base speed. The dynamic controller correlates much more closely to the maximum torque profile. Since the current regulators are held on the operational side of the saturation limit, unmodelled effects or parameter errors are catered for by the reserved voltage. Figure 8 shows the experiment repeated

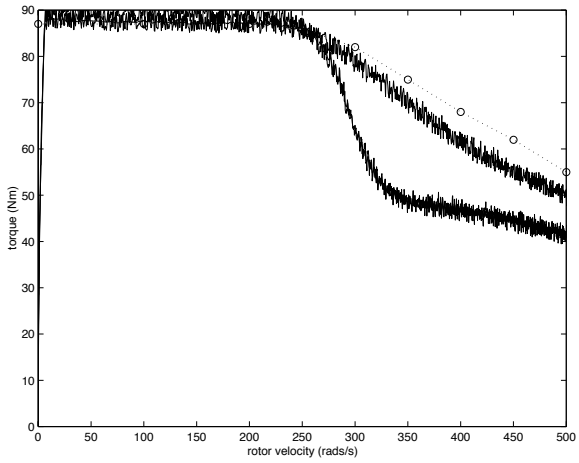

Figure 8: Experimental torque profiles of the steady state and dynamic controllers, compared to the maximum achievable torque profile, rotor only load.

with the motor disconnected from the external load. In both cases the maximum achievable torque profile has been calculated from the steady state system equations. The steady- state controller performance drop is even more pronounced in this case due to the reduced system inertia which results in an increased rate of current vector advance. Again, the dynamic controller correlates closely to the predicted maximum torque speed envelope. The magnitude of the applied voltage can be measured directly from the DSP board outputting the PWM signals to the inverter. The PWM synthesiser is supplied with modulation depth commands which are translated into three phase PWM signals. The magnitude of the applied voltage can therefore be calculated from the measurement of dc link voltage and the depth of modulation. Examination of figure 9 reveals the predicted action of the dynamic and steady state controllers. At the boundary with the field weakening region, the steady state current controllers saturate, and the applied voltage is subject to a PWM modulation depth of 100%. The dynamic controller operates just within the saturation limit, and thus maintains control of the current vector at all times throughout the operating range of the motor.

6 Conclusion

A model reference controller has been designed with a nonlinear representation including the constraints of the system. Without the inclusion of these constraints, the PI regulators saturate and current control is lost. The constraints when applied to the

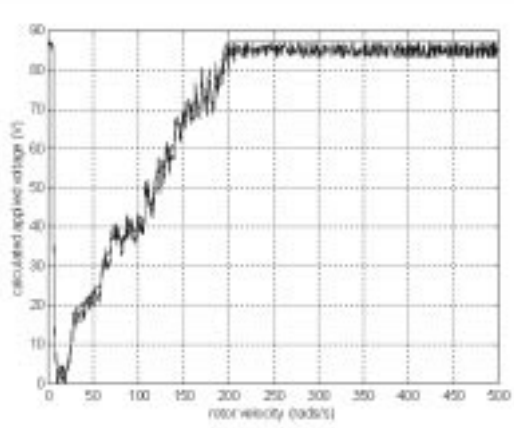

Figure 9: Applied voltage magnitude, experimental comparison of dynamic and steady state controller.

model reference controller allow the PI current regulators to accurately track the model reference command values, an achieve an optimal torque speed trajectory.

References

[1] T.M.Jahns, G.B.Kliman, and T.W.Neumann, "Interior permanent magnet synchronous motors for adjustable speed drives", *IEEE Trans. Ind. Appl.,* vol. IA-22, pp 738-747, July/Aug. 1986.

[2] P.Pillay, and R.Krishnan, "Modeling, simulation, and analysis of permanent magnet motor drives. Part I: The permanent-magnet synchronous motor drive", *IEEE Trans. Ind. Appl.,* vol. IA-25, pp 265-273, March/April. 1989.

[3] T.M.Jahns, "Flux-weakening regime operation of an interior permanent-magnet synchronous motor drive", *IEEE Trans. Ind. Appl.,* vol. IA-23, pp 681-689, July/Aug. 1987.

[4] R.Dhaouadi, and N.Mohan, "Analysis of current-regulated voltage-source inverters for permanent magnet synchronous motor drives in normal and extended speed ranges", *IEEE Trans. on Energy conversion,* vol. 5, no.1, pp 137-144, March. 1990.

[5] W.L.Soong, and T.J.Miller, "Field-weakening performance of brushless synchronous AC motor drives", *IEE Proc.-Electr. Power Appl.,* vol. 141, no.6 pp 331-339, November 1994.

[6] S.D.Sudhoff, K.A.Corzine, and H.J.Hegner, "A flux-weakening strategy for current-regulated surface-mounted permanent-magnet machine drives", *IEEE Trans. on Energy Conversion,* vol. 10, no.3 pp 431-437, September 1995.

[7] S.Morimoto, M.Sanada, and Y.Takeda, "Wide-speed operation of interior permanent magnet synchronous motors with high-performance current regulator", *IEEE Trans. Ind. Appl.,* vol. IA-30, no.4, pp 920-926, July/Aug. 1994.

[8] S.R.Macminn, and T.M.Jahns, "Control techniques for improved high-speed performance of interior PM synchronous motor drives", *IEEE Trans. Ind. Appl.,* vol. IA-27, pp 997-1004, Sept./Oct. 1991.

[9] C.C.Chan, J.Z.Jiang, W.Xia, and K.T.Chau, "Novel wide range speed control of permanent magnet brushless motor drives", *IEEE Trans. on Power Electronics,* vol. 10, no.5, pp 539-546, September 1995.

[10] S.D.Sudhoff, K.A.Corzine and H.j.Hegner, "A flux- weakening strategy for current regulated surface mounted permanent magnet machine drives", *IEEE Trans. on Energy Conversion*, vol.10, no.3, pp 431-437, September 1995.

[11] T.M.Jahns, G.B.Kliman, T.W.Neumann, "Interior permanent magnet synchronous motors for adjustable speed drives", *IEEE Trans. Ind. App.*, VOL.1A-22, NO.4, July/August 1986.

[12] T.M.Jahns, "Flux weakening regime operation of an interior permanent magnet synchronous motor drive", *IEEE Trans. Ind Appl.* VOL.1A-23, NO.4, July/August 1987.

[13] P.Stewart and V.Kadirkamanathan, "On steady state and dynamic performance of model reference control for a permanent magnet synchronous motor", *UKACC International conference on control '98, Swansea, U.K.* No.455, pp 664-669, IEE 1998, 1-4 September 1998.

[14] T.J.E. Miller, "Brushless permanent magnet and reluctance motor drives", University Press, 1993.

[15] P.Stewart and V.Kadirkamanathan, "Dynamic control of permanent magnet synchronous motors in automotive drive applications", *1999 American Control Conference, San Diego, USA*, IEEE 1998, pp 1677-1681, June 2-4, 1999.